Chemical Characterization of Microplastic Particles Formed in Airborne Waste Discharged from Sewer Pipe Repairs

Journal:	*Environmental Science: Processes & Impacts*
Manuscript ID	EM-ART-05-2023-000193.R2
Article Type:	Paper

Chemical Characterization of Nanoplastic Particles Formed in Airborne Waste Discharged from Sewer Pipe Repairs

Brianna N. Peterson,[1] A.C. Morales,[1] J.M. Tomlin,[1] C.G.W. Gorman,[1] P.E. Christ,[1] S.A.L. Sharpe,[1] S.M. Huston,[1] F.A. Rivera-Adorno,[1] B.T. O'Callahan,[3] M. Fraund,[4] Y. Noh,[5] P. Pahari,[5] A.J. Whelton,[5,6] P.Z. El-Khoury,[7] R.C. Moffet,[4] A. Zelenyuk,[8] A. Laskin.* [1,2]

[1]Department of Chemistry, [2]Department of Earth, Atmospheric and Planetary Sciences, Purdue University, West Lafayette, IN, USA

[5]Environmental Molecular Sciences Laboratory, [7]Physical Sciences Division, [8]Atmospheric Sciences and Global Change Division, Pacific Northwest National Laboratory, Richland, WA, USA

[4]Sonoma Technology, Inc., Petaluma, CA, USA

[5]Lyles School of Civil Engineering, [6]Department of Environmental and Ecological Engineering, Purdue University, West Lafayette, IN, USA

Environmental Significance Statement

Microplastic particles are inadequately characterized pollutants that harm the aquatic and atmospheric environments. Even if from the same emission source, microplastic particles of varying sizes are often different with respect to their composition, chemical reactivity and emission mechanisms. This work characterizes individual microplastic particles related to emissions from commonly used technology of trenchless cured-in-place-pipe repairs. Multi-modal particle characterization demonstrates substantial differences between particles of different sizes, indicating their different formation and aging mechanisms.

Chemical Characterization of Microplastic Particles Formed in Airborne Waste Discharged from Sewer Pipe Repairs

Brianna N. Peterson,[1] A.C. Morales,[1] J.M. Tomlin,[1] C.G.W. Gorman,[1] P.E. Christ,[1] S.A.L. Sharpe,[1] S.M. Huston,[1] F.A. Rivera-Adorno,[1] B.T. O'Callahan,[3] M. Fraund,[4] Y. Noh,[5] P. Pahari,[5] A.J. Whelton,[5,6] P.Z. El-Khoury,[7] R.C. Moffet,[4] A. Zelenyuk,[8] A. Laskin.* [1,2]

[1]Department of Chemistry, [2]Department of Earth, Atmospheric and Planetary Sciences, Purdue University, West Lafayette, IN, USA

[5]Environmental Molecular Sciences Laboratory, [7]Physical Sciences Division, [8]Atmospheric Sciences and Global Change Division, Pacific Northwest National Laboratory, Richland, WA, USA

[4]Sonoma Technology, Inc., Petaluma, CA, USA

[5]Lyles School of Civil Engineering, [6]Department of Environmental and Ecological Engineering, Purdue University, West Lafayette, IN, USA

Revised Manuscript for resubmission to

Environmental Science: Processes & Impacts

September 13, 2023

Abstract

Microplastic particles are of increasing environmental concern due to the widespread uncontrolled degradation of various commercial products made of plastic and their associated waste disposal. Recently, common technology used to repair sewer pipes was reported as one of the emission sources of airborne microplastics in urban areas. This research presents results of the multi-modal comprehensive chemical characterization of the microplastic particles related to waste discharged in the pipe repair process and compares particle composition with the components of uncured resin and cured plastic composite used in the process. Analysis of these materials employs complementary use of surface-enhanced Raman spectroscopy, scanning transmission X-ray spectro-microscopy, single particle mass spectrometry, and direct analysis in real-time high-resolution mass spectrometry. It is shown that the composition of the relatively large (100 μm) microplastic particles resembles components of plastic material used in the process. In contrast, the composition of the smaller (micrometer and sub-micrometer) particles is significantly different, suggesting their formation from unintended polymerization of water-soluble components occurring in drying droplets of the air-discharged waste. In addition, resin material type influences the composition of released microplastic particles. Results are further discussed to guide the detection and advanced characterization of airborne microplastics in future field and laboratory studies pertaining to sewer pipe repair technology.

Introduction

Since the 1950s, the global production of plastic has increased from 2 million to 460 million metric tons per year.[1,2] Degradation of plastic installations and discarded waste by pathways that include sunlight, water, and biogeochemistry, to name a few, results in the formation of microplastic[3–5] debris, which can further degrade to form smaller nanoplastic[6] particles. Additionally, microplastic particles are in production as engineered commercial materials used in cosmetics, paints, composite materials, etc.[7,8]

Microplastics of smaller sizes are more labile in the environment and undergo faster and more long-range transport through air and water.[9,10] Smaller microplastic particles also have higher surface-to-volume ratios, resulting in their higher reactivity and susceptibility to environmental weathering.[6,9] This results in diverse variability and significant differences in the chemical composition of microplastic particles of different sizes, as they continue to evolve in the environment.[11,12] Microplastics adversely affect the overall health of ecosystems, biological organisms, and humans, making them critical to study.[13–15] Most frequently, observations of microplastic have been reported for aquatic, marine, and terrestrial environments, but recent studies showed that they also become airborne due to wind and other mechanical forces.[16–20] Notably, long-range atmospheric transport of microplastics has been confirmed by their observations in snow deposits at remote, high-altitude mountain sites.[21–23]

Microplastics of few millimeters in size were identified as an environmental concern before smaller (micrometer and sub-micrometer) particles and therefore more analytical methods have been adopted for routine characterization and quantitative analysis of large microplastics, such as Fourier transform infrared spectroscopy (FTIR), Raman spectroscopy, and pyrolysis gas-chromatography mass spectrometry.[24,25] Because of their minute amount of analyte and varied composition, smaller microplastic particles pose many analytical challenges for their detection and characterization.[26,27] Sizes of microplastic particles can be inferred from light scattering techniques and their morphology can be imaged by optical and electron microscopy. However, characterizing chemical composition of the micrometer and sub-micrometer microplastic is more challenging.[27,28] Traditional Raman and FTIR spectroscopy possess spatial resolution limits that make it difficult to characterize individual particles of the sub-micrometer sizes.[26,29] Mass spectrometry measurements are sensitivity limited as well due to small sample size and therefore require additional steps in sample preparation, such as sample digestion or pre-concentration.[30] Recently, thermal desorption – proton transfer reaction – mass spectrometry has offered promising results for microplastic characterization.[22,31,32] This method has both high sensitivity and high mass resolution, enabling the use of small sample sizes and accurately characterizing many types of polymers. However, it uses bulk microplastic samples and does not offer information on individual particles.[31] Characterization of microplastics also becomes complex if the sample is present within a complex organic matrix or if the plastic has aged or oxidized.[33] To gain comprehensive insights on both single particle and bulk molecular properties of microplastics, multiple modes of detection are needed.

A potentially important source of direct airborne emissions of microplastic particles has been attributed to a commonly used technology to repair storm and sanitary sewer systems, known as cured-in-place-pipe (CIPP) installations.[34] This trenchless technology involves inserting a resin-impregnated tube liner into a damaged pipe, inflating the liner against the pipe walls by pressurized air, followed by polymerizing (curing) the resin initiated by heat or ultraviolet (UV) light.[35,36] While this repair technology is cost efficient and has become common municipal practice, significant emissions of microplastic by the air-discharged steam-laden waste was recently reported.[34] In that study, chemical characterization of the waste condensates collected at installation sites employing styrene-based resin (associated with elevated levels of volatile organic compounds, VOC) and vinyl ester-based resin (alternative material designed to limit emissions only by low volatility organic compounds, LVOC) was performed.[34] Polymer precursors and other low-volatility organic species were identified as components of microplastic. Observed microplastic particles of larger sizes indicated spectral signatures consistent with polymers comprising resin material, such as polystyrene, styrene maleic anhydride, polydimethylsiloxane, polymethyl methacrylate, etc. In contrast, the composition of the sub-micrometer particles with viscoelastic properties resembling those of microplastic appeared to be more complex, and they showed little to no resemblance with the original resin material. It has been concluded that these sub-micrometer waste particles are formed through environmental oligomerization reactions of various soluble organic species present in drying droplets of the discharged waste.[34]

To further understand the mechanism leading to formation of these highly viscous micrometer and sub-micrometer particles, this study systematically characterizes materials used in sewer pipe repair technology and compares the results with the composition of microplastics attributed to the field-collected waste condensates. An array of complementary analytical techniques is employed for comprehensive analysis of microplastics, including surface-enhanced Raman spectroscopy (SERS), scanning transmission X-ray microscopy (STXM), single particle mass spectrometry (miniSPLAT), and direct analysis in real-time high-resolution mass spectrometry (DART-HRMS). We compare the composition of microplastic particles to determine their origin in the emissions. Our results suggest that the large particles are primary emission fragments of the cured material, which become airborne during the installation procedure. In contrast, the micrometer and sub-micrometer particles are a unique type of secondary organic aerosol formed by aqueous-phase oligomerization reactions in drying droplets of the discharged waste. Notably, the resin composition is also an important factor in defining the composition of directly emitted and secondary formed microplastic particles, highlighting the need for further systematic evaluation of multi-phase emissions from this widely used technology.

Experimental Methods

Microplastic particle samples. Samples of the discharged waste condensates were collected from sewer pipe repair installations in Sacramento, CA, using cold traps.[37] Waste samples used in this study were collected from two installations, one using a styrene-based (S-based) resin and the other using a “styrene-free” vinyl ester-based (VE-based) resin. Matching materials used in these installations, commercially available S-based and VE-based resins were obtained. The cured composites were generated by mixing each of the two resin types with peroxide initiators (Perkadox®26 and Luperox®P for the S-based resin and cumene hydroperoxide for the VE-based resin) and applying the mixture to polyester felt (Model# 24-125 PE, Sutherland Felt Company, MI, USA). The resin saturated felt was then cured in a thermally based curing system.[38] The S-based resin was cured for 50 minutes at a temperature of 65.6 °C, while the VE-based resin was cured for 30 minutes at 82.2 °C.[38] The curing time and temperature were based on manufacturer guidelines. Further information about sample collection is included in Supplementary Information Note 1.

Particles generated from the collected waste condensates ranged from 0.02 to 10 μm in size. The detailed particle size distributions (PSDs) of both aerosolized dry particles and insoluble colloids present in the waste samples have been quantified and reported in our previous work.[34] The $\Delta M/\Delta logD_p$ PSDs showed mean sizes of the dry particles and the wet colloids in the sub-micrometer and the above-micrometer ranges, respectively. The total organic carbon (TOC) mass loadings in the waste samples were reported in the range of 13-133 mg/L.[34] Given the wide range of particle sizes observed, it became evident that a comprehensive approach utilizing complementary analytical techniques capable of characterizing particles across various size ranges was necessary.[34] A multi-modal characterization approach was employed in this study to provide description of the microplastic particles with both single-particle and molecule-specific levels of detail.[39] Figure 1 outlines an overview of the sample preparation and the experimental methodology used for this study.

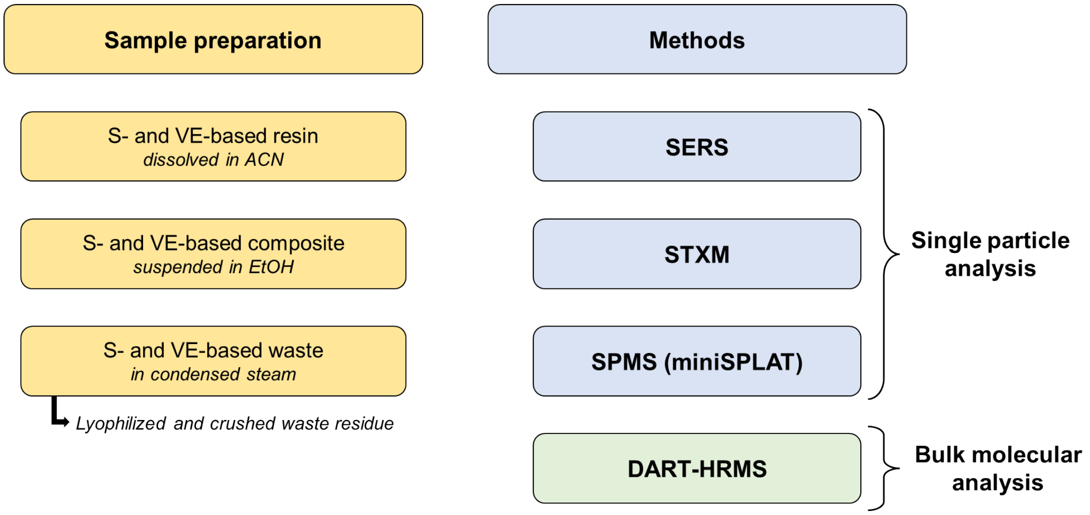

Figure 1. An overview of the sample preparation and experimental methods used in this study. Acronyms in the figure indicate: Styrene-based (S-based); vinyl ester-based (VE-

based); surface enhanced Raman spectroscopy (SERS); Scanning transmission x-ray microscopy (STXM); single particle mass spectrometry (SPMS); direct analysis in real time high resolution mass spectrometry (DART-HRMS).

Acetonitrile laden microplastic particles were prepared by dissolving each of the S-based and the VE-based resins in acetonitrile to form a colloidal solution. Acetonitrile was chosen as other solvents tested resulted in the aggregation of resin rather than suspension of small particles throughout the solution. The cured composites were first powdered using a mortar and pestle. This was done by cutting smaller pieces of a large composite block and then grinding them as is in a ceramic mortar and pestle until they were a fine powder. The powdered composite was then suspended in ethanol to prepare colloidal solution ready for particle generation through nebulization. The waste samples contained dissolved materials and colloids already suspended in the aqueous slurries.[34]

Different preparations of the microplastic samples were needed depending on the analytical technique used. For the SERS analysis, samples were prepared by drop-casting of colloidal solutions onto SERS substrates and allowing them to dry. Lyophilized waste materials were prepared by cryodesiccation of the waste condensates and crushing obtained dry material into smaller particles. This allowed for the creation of larger (100 μm) sized particles that represented the bulk composition of the waste material. For STXM analysis, sample solutions were atomized using a medical nebulizer, obtained aerosol was dried to 18% relative humidity (RH) using dry N_2 and silica gel, and dry particles were impacted using a Sioutas impactor (Stage C) onto silicon nitride windows. The nebulizing flow rate was set at 2.1 L/min and the carrier gas flow was maintained between 9-10 L/min. For miniSPLAT analysis, samples were atomized and dried to ~20% RH, then passed through a charcoal filter to remove any additional VOCs. Then, the dried particles were introduced into a 100 L Teflon bag that had been pre-filled with 60 L of clean, dry air to minimize particle coagulation and further dry the aerosols sample (~5% RH). For the DART-HRMS analysis, no further sample preparation was needed.

Chemical imaging of substrate-deposited particles. Glass slides sputter-coated with 50 nm of Au with nanoscale roughness (~5 nm) were used as substrates for SERS analysis. The gold coating enhances detection sensitivity by enhancing the incident and scattered radiation from analytes in the immediate vicinity of the metal. Samples were deposited on the SERS substrate as described in Supplementary Note 2. Single particle Raman measurements were taken using a 785 nm laser with a confocal Raman microscope. Spectral features were identified using the Wiley KnowItAll™ Raman spectra software and compared to literature spectra of polymer standards.[40–43]

STXM-NEXAFS (near-edge X-ray absorption fine structure spectroscopy) analysis was performed at the Advanced Light Source synchrotron facility of Lawrence Berkeley National Laboratory. Particles deposited onto silicon nitride thin film substrates were raster scanned through focused X-ray beam at energy levels from 278 to 320 eV to generate spectral images (Supplementary Information Note 2). Transmitted light is converted into optical density via Beer's law and plotted to construct NEXAFS spectra. Spectral analysis is done through MATLAB scripts that differentiate types of carbon based on its characteristic NEXAFS features.[44–48] Approximately ~80 particles for each of the six samples (resin, composite, and waste for the S-based and VE-based systems) were analyzed with STXM during the course of this study.

Real-time characterization of individual aerosolized particles. The information provided by STXM is invaluable for microplastic characterization. However, time limits and facility access constraints lead to a limitation on the number of particles that can be analyzed. High-throughput analysis by the single particle mass spectrometer, miniSPLAT, was employed for further characterization of particles with substantial statistical depth, by measuring size and mass spectra for thousands of individual particles.[49] Specific details of the miniSPLAT instrument and its operation were published elsewhere[49] and briefly summarized in Supplementary Information Note 3. Sample solutions were atomized using a medical nebulizer with an airflow of 5 L/min through charcoal and silica gel filters to reduce VOCs and moisture. The dried particles were added for ~ 4 min to a 100 L Teflon bag pre-filled with 60 L of clean dry air and sampled by miniSPLAT until approximately 5,000-10,000 single particle mass spectra were acquired.

Molecular characterization of bulk samples. DART is an ambient ionization source that desorbs and ionizes gas-phase analyte by collisions with hot excited He gas. It requires little to no sample prep, making it advantageous to use for bulk molecular characterization of microplastic.[50] Specific details on the DART source operation and ionization mechanisms are included in Supplementary Information Note 4. Briefly, two sample introduction methods were used for DART-HRMS experiments in this study to detect a broader range of compounds in the samples. In the first method, the linear rail with the QuickStrip attachment was used (Figure S3a).[51] This consists of a paper card with 12 metal mesh sample spots on it. Sample solutions are dropped on each spot and allowed to dry before being placed in the linear rail which moves the card across the DART source at a programmed speed. The gas temperature used by the DART source was changed throughout the method, enabling the ionization of different compounds as temperature increased. In the second method, the BioChromato IonRocket heating stage was used (Figure S3b).[52] This method heats the sample placed into a copper pot along a computer-programmed temperature gradient. As the sample is heated, different chemical species are desorbed and then ionized by the DART source.

The DART source was the Ionsense Jumpshot with a VAPUR® interface coupled to a high-resolution Orbitrap mass spectrometer (Q Exactive HF-X, ThermoFisher Scientific, Inc.). Helium gas was used as the ionization gas, while N_2 flowed through the source while the instrument was in standby mode. For experiments using the linear rail, 5 µL of each respective sample was spotted on eight of the twelve available spots on the mesh card. The remaining four spots received 5 µL of the relevant solvent for each of the sample types (resin – acetonitrile; composite – ethanol; waste – water). The samples were allowed to dry and then placed in the DART linear rail attachment. Helium gas was pulsed for 3 seconds on each sample with a 2 s next sample delay, and a 30 s heater wait time. Gas temperature was set at 150°C, 250°C, 350°C, and 450°C. This allowed one blank and two sample spectra to be taken at each gas temperature. For experiments using the IonRocket heating stage, 5 µL of the sample was placed into a copper pot. The latter was installed on the IonRocket sample holder, and then heated using a programmed temperature gradient of a 30 second temperature hold at 50°C, a ramp up to 600°C at a rate of 150 °C/min and then a 30 second hold at 600°C. The DART-HRMS datasets were processed as described in previous studies outlined in Supplementary Information Note 4.[53]

Results and Discussion

The resin used in sewer pipe repairs is cured by radical initiated polymerization (illustrative reaction schemes and corresponding discussion are included in Supplementary Information Note 5).[54] Thus, chemical composition of the polymerized resin (composite) is representative of the intended polymerization mechanism for the system. If the airborne microplastic particles observed in the waste were the degradation debris shed from curing composite material, they would resemble the resin and composite composition. However, if the microplastic particles were formed as unintended polymerization through various oligomerization reactions in the evaporating waste droplets, as previously proposed,[34] they would not bear a resemblance to the resin or composite.

SERS is a commonly used method for characterizing microplastics, for which many spectral databases have been created to identify common polymers.[29] Figure 2a shows the spectra of a polystyrene (PS) standard compared to the S-based resin, corresponding composite, and examples of large lyophilized waste particles. Figure 2b shows the same for the VE-based resin, composite, and waste lyophilized particles in comparison to ethoxylated bisphenol A (BPA). The dashed lines show similarities between the spectra for each feature. Representative PS features observed across all the samples are located at 614 cm^{-1} (C-C stretch), 1000 cm^{-1} (breathing mode of the aromatic ring), 1154 cm^{-1} and 1435 cm^{-1} (bending of aromatic C-H), 1602 cm^{-1} (C=C stretch), 2868 cm^{-1} and 2931 cm^{-1} (*sym* and *asym* stretching modes of aliphatic C-H, respectively), and 3075 cm^{-1} (stretching of aromatic C-H).[34,40,41] For the S-based particles, MP particles share many features with the resin and the composite (Figure 2). This indicates that the S-based large (~100 μm) lyophilized waste particles are most likely fragments of the composite shed during the curing process.

Spectra of the VE-based particles are more complex. The VE-based particles share features at 614 cm^{-1} and 1000 cm^{-1} that potentially could be contributions from PS. Contamination of the intended "styrene-free" resin by PS has been reported prior.[37,38,55] The VE-based particles also share many spectral features with ethoxylated bisphenol-A.[40] This includes peaks at 641 cm^{-1} (aromatic stretch), 819 cm^{-1} (C-H out of plane bend), 1111 cm^{-1} (C-H-bending), 1191 cm^{-1} (vinyl stretch), 1234 cm^{-1} (CO stretch and C-C stretch in both rings),1290 cm^{-1} (C=C stretching in both rings), 1451 cm^{-1} (CH_3 bending), 1615 cm^{-1} (C=C stretching in both rings), and 2942 cm^{-1} (OH stretch).[43] Vinyl ester-based resins are created by the esterification of an epoxy resin (such as bisphenol-A) and acrylic or methacrylic acids (Supplementary Information Note 5).[42] While the VE-based features cannot be attributed solely to ethoxylated BPA, there are still several similarities between particles generated from resin, composite, and lyophilized waste material. This suggests that in the VE-based system large (~100 µm) lyophilized waste particles also originate from the cured composite material.

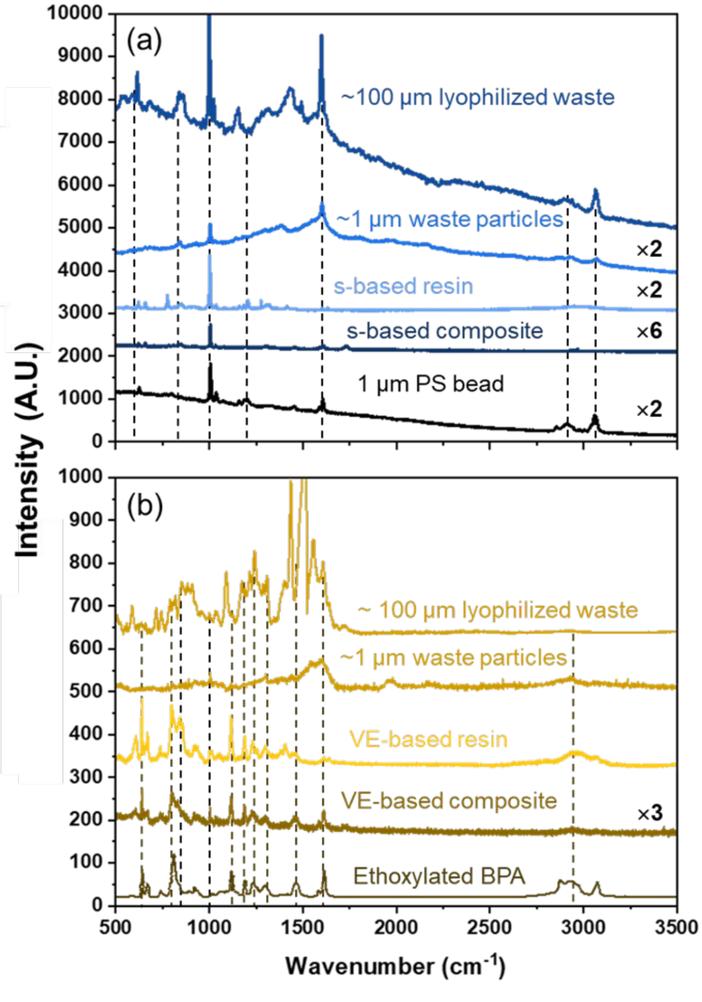

Figure 2: (a) SERS spectra of a 1 µm PS bead, S-based composite, S-based resin, 1 µm waste particles, and 100 µm waste particles and (b) SERS spectra of ethoxylated BPA, VE-based composite, VE-based resin, 1 µm waste particles, and 100 µm waste particles. For visual comparison, selected spectra are scaled up as indicated by the scaling factors

placed above the spectral lines. Dashed lines indicate features shared between the samples. SERS spectra of waste particles have been previously shown in Morales et al. (2022).[34]

Because of its higher spatial resolution, we employed STXM-NEXAFS for the analysis of the micrometer and smaller particles.[56] Figure 3 illustrates the STXM spectra of particles generated from the S-based and VE-based resins, composites, and wastes. Dashed lines show features corresponding to carbon functional groups: C*=C (285.2 eV), C*=O (286.7 eV), C*H (287.7 eV), C*OOH (288.5 eV), C^*O_3 (290.4 eV).[30] A prominent alkene feature (285.2 eV) is present in the PS bead, S-based composite, and resin; however, it is not present in the waste. In contrast, the waste particles have intense features from the carbonyl (286.7 eV) and carboxylic acid (288.5 eV) functional groups that are not present in the other samples. Unlike the large lyophilized waste particles, the waste particles of micrometer sizes do not resemble their corresponding resin or composite material. PS, the intended product of polymerization consists of mostly sp^2 carbon and contains no carbonyls or carboxylic acids. Detection of carbonyl and carboxylic acid features in the micrometer waste particles suggests that they are formed through alternative polymerization mechanisms.

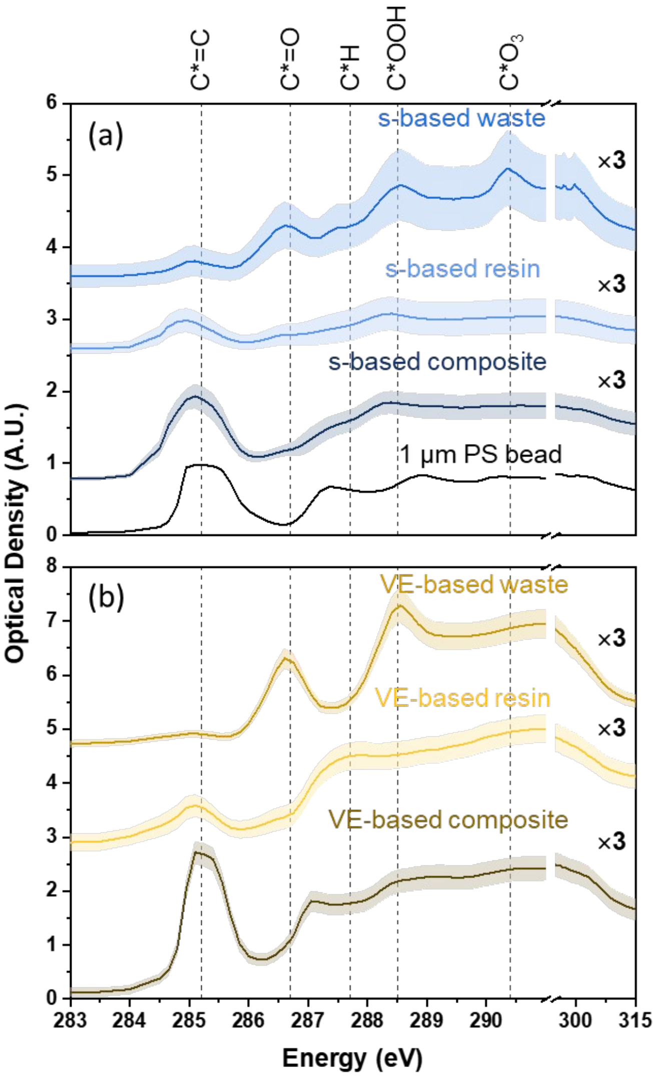

Figure 3: Average STXM-NEXAFS spectra of (a) a 1 µm PS bead, S-based composite, S-based resin, and S-based waste and (b) VE-based composite, VE-based resin, and VE-based waste. To facilitate visual comparison, signals were multiplied by the number indicated above the spectral lines. Shaded regions represent variability in spectra and dashed lines indicate features from specific functional groups.

The same difference is observed between the VE-based waste particles (Figure 3b) and their corresponding resin and composite materials. The VE-based resin and composite have prominent alkene spectral features (285.2 eV), which are not present in the waste material. The waste particles, however, contain strong carbonyl and carboxylic acid features, which are not present in the resin or composite. In contrast to the VE-based large lyophilized particles, particles of micrometer sizes do not resemble the composition of the resin or cured composite material. The common differences between the large lyophilized and small micrometer particles indicate two things. First, between the two types of resin used (S- and VE-based), the particles have different composition indicating that the resin composition does have an impact on the makeup of discharged waste. Second, the disparity between large and small waste particles within each of the two sample sets (S- and VE-based) suggests that the small particles are formed by a different mechanism in steam-laden emissions, while the large particles are fragments of the cured resin/composite shed by mechanical forces experienced during curing.

This difference in composition is further evident from the internal heterogeneity of particles. Figure 4 displays the NEXAFS maps of individual micrometer and sub-micrometer particles from each of the six samples indicating the spatial distribution of different carbon functionalities. Particles are colored by the material present as defined by the thresholds as outlined in prior studies and Supplementary Information Note 2. Green represents organic carbon, red represents sp^2 hybridized carbon, and blue represents inorganic material.[45–48,57] As indicated by the maps, both the S-based resin and composite particles (Figs 4a-c) contain a large amount of sp^2 hybridized carbon in the center with some contributions from carboxylic organic carbon on the outer particle areas. In contrast, the waste particles predominantly consist of evenly distributed carboxylic organic carbon occasionally mixed with inorganic components.

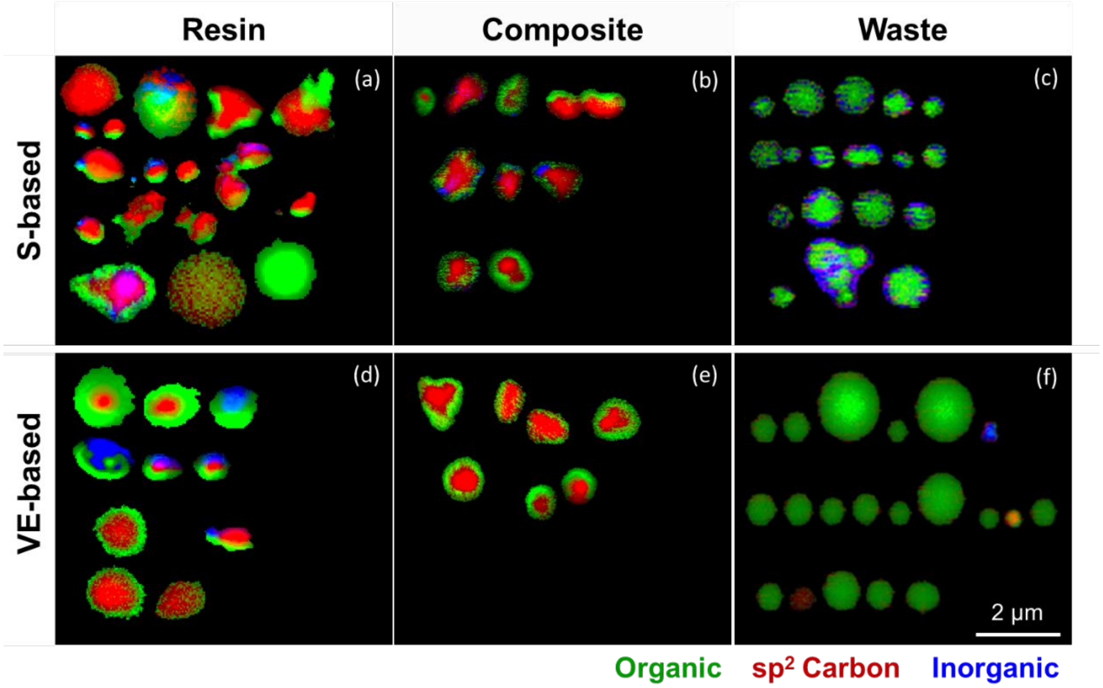

Figure 4: STXM-NEXAFS particle maps of the S-based (a) resin, (b) composite, and (c) waste and the VE-based (d) resin, (e) composite, and (f) waste. All are scaled to the scale bar in the bottom right corner. Organic carbon is represented by green, sp^2 hybridized carbon by red, and inorganic material by blue.

Maps of the VE-based particles (Figs 4d-f) are similar to the S-based particles and again are reflective of their corresponding NEXAFS spectra. The resin and composite particles are both mostly sp^2 hybridized carbon in the center with some organics in the outer areas, while the waste particles are almost entirely organic. The difference in composition between the resin and composite materials to the waste particles in both systems indicates that formation of the microplastic alike highly viscous waste particles is a process occurring outside of the intended polymerization.

To complement chemical imaging characterization results of individual particles with additional data and extensive statistical depth, we analysed large ensembles of individual particles using miniSPLAT. Due to significant fragmentation caused by laser ablation, the goal of processing miniSPLAT data is not to assign molecular formulas for detected peaks, but rather to compare mass spectral signatures across the samples to examine the presense of common peaks. Figure 5 shows the average particle mass spectra for each of the six sample types.

For the S-based resin and composite particles (Figure 5a, b), there are several mass spectral features shared between the samples, including (*m/z*=78 ($C_6H_6^+$), 92 ($C_7H_8^+$), 106 ($C_7H_6O^+$), 52 ($C_4H_4^+$), 42 ($C_3H_6^+$), 28 (CO^+). While the average mass spectrum of S-based waste particles (Figure 5c) shares some of these peaks; they are more complex and exhibit additional peaks. Even with sharing features, the overall shape and intensity of the spectral signature between the resin and composite and the waste are vastly different, indicating a difference in composition between those samples.

The same trend is seen for the VE-based waste particles where the VE-based resin and composite particles have similar spectral features which are not present in the waste material (Figure 5d, e, f). The VE-based resin and composite particles contain the same features at (*m/z*=114 ($C_6H_{10}O_2^+$), 70 ($C_4H_6O^+$), 42 ($C_3H_6^+$), while the waste particles exhibit very different mass spectra. The miniSPLAT data further reinforces that the composition of the particles in the waste material is different from the resin and composite. It also again displays the difference between the S-based and VE-based materials, indicating that the waste particles are newly formed in the waste emissions and their composition is different between the two cases.

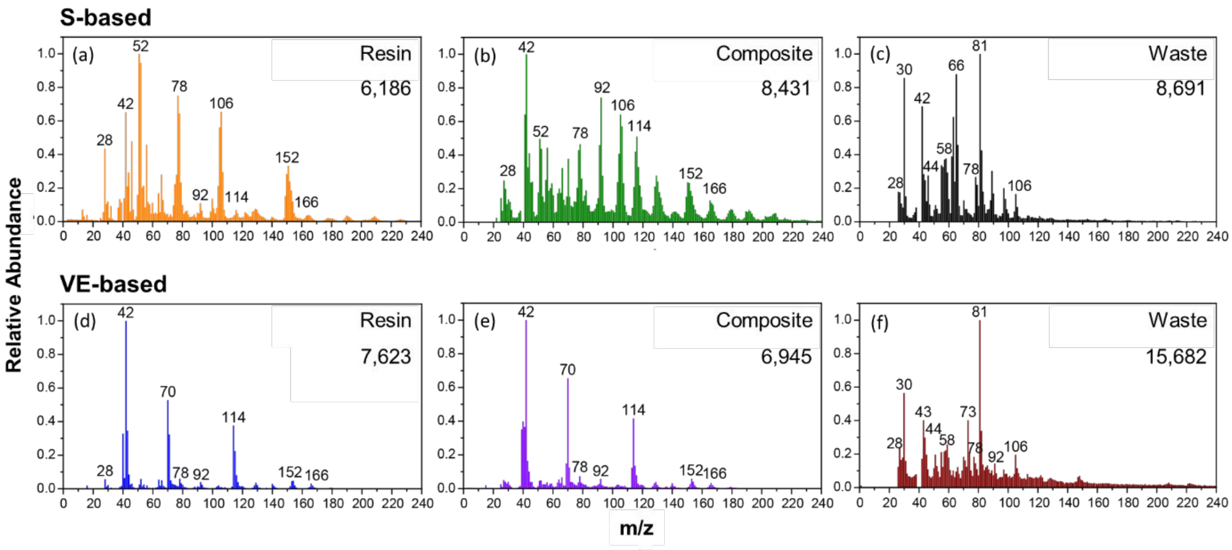

Figure 5: miniSPLAT-MS spectra of the S-based particles generated from (a) resin, (b) composite, and (c) waste and the VE-based particles generated from (d) resin, (e)

composite, and (f) waste. The number beneath the sample type represents the number of particles analyzed.

Mass spectra produced using DART-HRMS indicate molecular differences between composition of particles generated from resin, composite, and waste for both systems (Figure S7 and S8). Based on the accurate measured masses, up to ~80% of spectral features were assigned for each sample, for which number of assigned species varied in the range of 1400-4900 features. The composites contained the greatest number of detected species while the resin and waste of each respective system contained a similar number of detected compounds. Only 5-10% of species assigned were shared between all three samples (i.e., resin and composite, resin and waste, and waste and composite) (Figure S15). It follows that there are large compositional changes occurring as the resin is cured into composite and as waste is released. Furthermore, only 20-30% of the compounds assigned are shared between the two systems (i.e., S-based resin vs. VE-based resin) (Figure S16). This confirms that the type of resin used does impact the composition of waste particles formed and potentially the number of particles released. More research is needed in this area to fully understand the role of material in formation and release of waste microplastic particles.

Notably, there is a difference in ions detected using the linear rail DART experiment compared to the IonRocket experiment (Figure S17). Less than 1% of the HRMS features are shared between two experiments for each of the samples. This observation is consistent with previously reported differences in direct DART-HRMS analysis (linear rail) versus the temperature desorption DART-HRMS (IonRocket) employed for the characterization of polymers[51,58,59] This notable difference is rationalized by distinct mechanisms of the analyte desorption and introduction into the ionization zone of DART. In the direct DART-HRMS, the sample is placed directly in front of the DART source so the hot He gas desorbs and ionizes analyte components that can be rapidly volatilized by short pulses (3 sec) of the gas heated to 150-350 °C.[59] In contrast, the IonRocket heats the sample itself to much higher temperatures (50-600 °C) and at much longer experimental time (5 min), causing substantial thermal degradation (pyrolysis) of the polymer sample. In this case, ions detected by DART-HRMS are dominated by the pyrolysis products. Furthermore, variations in either the He gas temperature or the

IonRocket temperature ramp additionally influence the apparent mass spectra of the same analytes.[60] Nevertheless, both methods offer advantages for polymer analysis, depending on the goal of study. Experiments with slow and lowered temperature ramp using either the IonRocket or the direct desorption by pulsed heated gas facilitate preferential detection of the non-polymerized additives.[59] On the other hand, detection of the plastic pyrolysis products in the IonRocket experiments provides analyte-specific HRMS data indicative of the original polymer composition and therefore are beneficial as a method for rapid identification of plastic.[59,61,62] Within the context of this work, we combined results of both DART experiments for each of the analyzed samples to facilitate holistic comparison between their HRMS spectra.

Figure 6 shows the percent contribution of each elemental class across the samples, summarizing elemental assignments based on the DARTT-HRMS data (combined results of the direct and the IonRocket experiments). The general contributions of each of the classes are largely comparable across samples. CHO and CHON are the predominant classes making up 60-80% of each sample. The resin for both the S- and VE-based systems contained the greatest number of CHON species within both systems. The percent contribution of CHON decreases in cured composite and waste samples. Fractions of CHOS and CHONS classes (~10%) are somewhat smaller than those reported previously based on the ESI-HRMS and APPI-HRMS analysis of the solvent extracted samples.[63] This likely reflects the differences in ionization mechanisms between ESI, APPI, and DART.

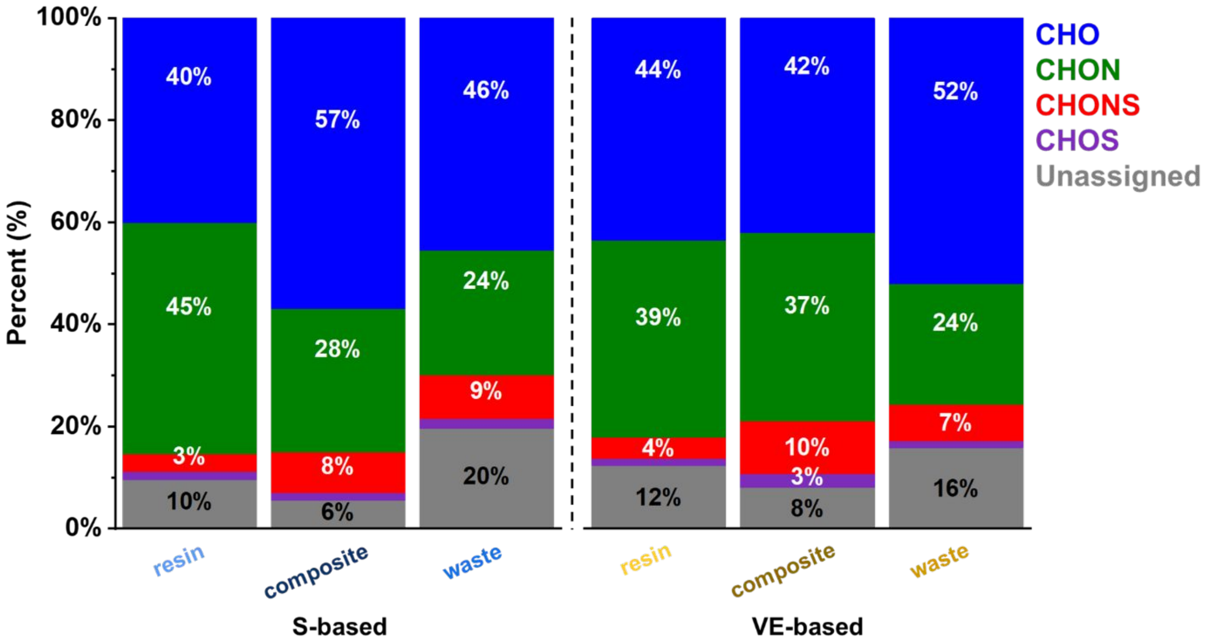

Figure 6. Percent composition of different elemental classes assigned based on the DART-HRMS data for each sample.

Selected polymer precursors, radical initiators, and compounds associated with initiator decomposition were identified in the mass spectra of the resin, composite, and waste.[34,63] A few polycyclic aromatic hydrocarbons (PAHs) and potentially oxidized derivatives were also identified. PAHs have been identified as a class of compound that can sorb to microplastic particles.[64] These are summarized in Table S1. All of these compounds have been previously identified in prior studies,[34,37,38,55,65,66] but this is the first time they have been systematically identified in both the S- and VE-based systems for the resin, composite, and waste. This is also the first study to comprehensively characterize each of these materials using DART-HRMS. Similarities of the compounds presented here based on the DART-HRMS data and the ESI- and APPI-HRMS results reported earlier[34,63] indicate that DART-HRMS provides comparable results. Therefore, application of DART-HRMS is especially advantageous for the analysis of the resin and composite samples as no additional sample preparation is needed.

Assessments of the individual species assigned based on the DART-HRMS data provide important insights into further understanding of the resin and composite composition. As seen in Table S1, many of the identified compounds were observed in each of the six samples (resin, composite, and waste for both the S- and VE-based systems). This indicates that while the overall mass spectra for each sample differ from each other in terms of their ion intensities, they still share many common features. The presence of plastic monomers and initiators in the composite and waste material suggests that even after curing there is still considerable amount of unpolymerized components that can be dissolved and washed out by the discharged steam. As water evaporates from the discharged steam droplets blown into the air, these dissolved components undergo unintended environmental oligomerization, which results in the formation of microplastic particles.[34]

Based on the formula assignments for individual species inferred from DART-HRMS data, several metrics of the analyzed materials are estimated and visually presented to further understand each sample (Supplementary Information Note 6). Plotting double bond equivalency (DBE) values against the number of carbon and nitrogen for each assigned species (Figure S9) allows the differences in composition and structure to be visualized. As expected, the resin samples for both systems fall more into the aliphatic region and contain compounds of lower DBE values, although the VE-based resin does have a larger number of compounds in the aromatic region compared to the S-based resin. As the resin cures, the DBE values increase as polymers are formed. The composite DBE plots reflect this as they contain compounds predominantly in the aromatic region. Interestingly, the waste sample DBE plots appear to be visually similar to the resin plots. The waste samples contain more aliphatic compounds and there is a difference between the S- and VE-based systems where the VE-based waste contains more aromatic species. The Van Krevelen diagrams shown in Figures S10-S11 indicate similar trends as the DBE plots.[67] For both systems, the resin and waste samples share more visual similarities than the waste to the composite. For the S-based system, the waste consists of many highly saturated and oxidized saturated species that are more aromatic, as seen in the DBE plots as well. The resin and waste contain contributions from oxidized aliphatic species. Whereas the S-based composite contained more aromatic species, the VE-based composite contains more aliphatic oxidized species. The composition of the VE-based resin and waste contains a more complex mixture of aliphatic and aromatic species with varying degrees of oxidation.

Many of the species identified are not heavily oxidized as indicated by their relatively low nominal oxidation state values (NOS_C)<0 (Figure S12), which are consistent with those previously reported for the waste samples based on the ESI/APPI-HRMS data sets.[63] Again, distribution of the NOSc values for the resin is visually similar to the waste with many species having low values of NOS_C <0. These more reduced (less oxidized) species have the potential to be oxidized in the presence of common atmospheric pollutants such as ozone, hydroxyl radicals, and NO_x. Atmospheric oxidation changes the chemical composition and causes reductions in volatility and corresponding increases in the viscosity of atmospheric particles.[68] This is due to the addition of more polar functional groups, such as aldehydes, ketones, or carboxylic acids. From the results of the mass spectra and STXM-NEXAFS (Figure 3), the waste particles do contain carboxylic acid and carbonyl-containing compounds which reduce their volatility and increase their viscosity.[69]

Using empirical parameterization models, volatility and viscosity of individual components were estimated based on their formula assignments (Supplementary Information Note 6).[70,71] Figure 7 shows box and whisker plot distributions of the estimated volatility of assigned compounds for each sample. Notably, the estimated volatility of the composite components is lower than those of the resin and waste. This makes sense as the composite is engineered to be a solid material. The resin components are the most volatile. While the VE-based system was engineered with the intent to produce fewer VOCs than the S-based system, there does not appear to be a large difference in their lower volatility components produced by either system. A majority of the species fall in the semi, low, or extremely low volatility categories (SVOC, LVOC, and ELVOC) for both systems (Figures S13-S14). Compounds of low volatility more readily partition into the condensed phase and form amorphous solid-particles such as microplastics.[69]

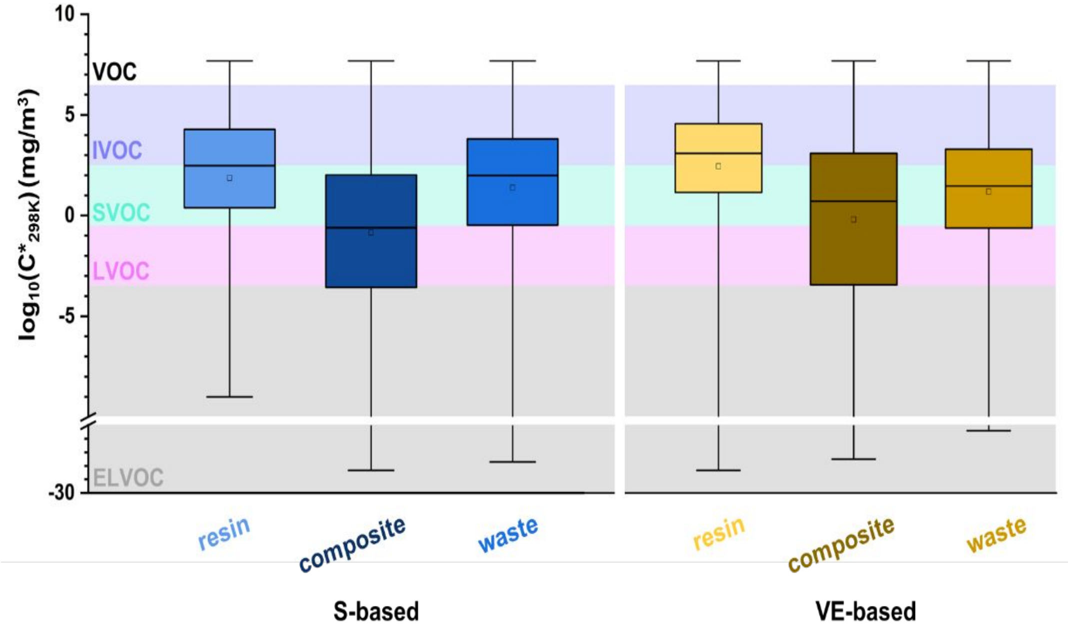

Figure 7. Box and whisker plot showing distributions of the estimated volatility values for the assigned compounds detected by the DART-HRMS. The square icons represent the mean of the distributions. The middle box line represents the median. The bottom and top lines composing the box represent the 25th and 75th percentile, respectively. The whiskers represent the range of the data.

Consistent with their low volatility, individual compounds identified in the resin, composite, and waste suggest high viscosity of the corresponding dry residues. Figure 8 shows box and whisker plot distributions of the estimated viscosity of the individual assigned species for each sample. Both the composite and waste materials have higher estimated viscosity than the resin. The resin has the lowest viscosity of the three sample types followed by the waste, and the composite. The composite, as it is engineered to polymerize into a solid material, is highly viscous. Viscosity estimates for individual components present in the waste fall into the semi-solid to solid phase (10^4-10^{15} Pa·s). The low volatility and high viscosity of the waste increase the favorability of forming solid microplastic particles, as individual compounds oligomerize in drying droplets of the discharged waste.[34]

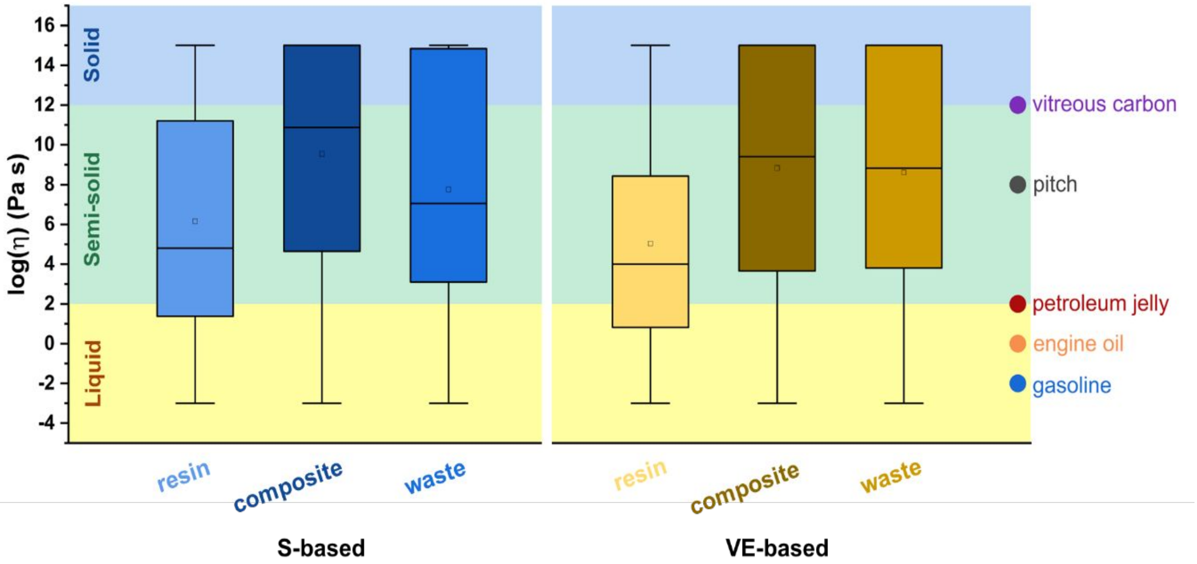

Figure 8. Box and whisker plots showing distributions of the estimated viscosity for the assigned compounds detected by the DART-HRMS. The square icons represent the mean of the distributions. The middle box line represents the median. The bottom and top lines composing the box represent the 25th and 75th percentile, respectively. The whiskers represent the range of the data.

Conclusions

The work done in this study confirms that the microplastic particles observed in sewer pipe repair systems are products of unintended polymerization in drying waste droplets. While the large debris material released during sewer pipe repair resembles the product of intended polymerization (the composite samples), the small micrometer and sub-micrometer particles do not follow this same trend. The difference in composition between large and small particles demonstrates that large microplastics are likely primary emitted fragments of the cured pipe aerosolized by the pressurized steam blown through the installation. The small microplastics, however, are likely secondary formed by oligomerization reactions of soluble organic species washed out by the steam from curing mixture. Several potential oligomerization reaction pathways have been proposed (Supplemental Information Note 5).[34] This includes esterification, aldol condensation, and acetal formation, to name a few.[34,72–77] The presence of low volatility and high viscosity compounds in the waste favor the formation of microplastic particles as the droplets dry.

Understanding the physicochemical properties of these materials is also crucial for further understanding their atmospheric fate[78,79] and their potential health effects.[80] Particle viscosity influences their response to relative humidity and temperature, which in turn impact aerosol growth and evaporation.[78,81] In low-viscosity particles, reactions of gas-particle oxidation and photochemistry occur rapidly and throughout the bulk of the particle.[78,82] In contrast, highly viscous particles undergo slower reactions limited to the surface layer.[83] Cloud formation is another facet of atmospheric chemistry that is influenced by particle viscosity.[78] Both cloud condensation nuclei (CCN) and ice nucleating particles (INP) are critical in the formation of clouds and their study is important for the impact of clouds on climate and precipitation patterns.[84] While microplastic particles are expected to have inhibited CCN propensity due to their surface hydrophobicity, the altered composition of aged microplastics increases their potential as CCN.[85] Good INP are typically described by their solid surfaces and do include highly viscous glassy organic aerosols.[86] Microplastic particles described here fit within this category as well.[85] Since the detection and impact of microplastics in the atmosphere is still in its infancy, examining their role as potential INP particles is an important topic to consider.[85]

By employing a combination of analytical techniques in this study, we have gained valuable insights into the microplastic particles generated during the CIPP repair process, both at the single particle and bulk molecular level. Understanding both the physical properties (size, morphology and viscosity) and chemical composition of these microplastic particles is crucial for assessment of their mobility, reactivity, toxicity, and many other properties.[87] MiniSPLAT proved to be particularly powerful in this study, as it provided characterization of large ensembles of particles. Furthermore, field-deployable miniSPLAT and similar single particle mass spectrometry techniques hold promise for future studies of airborne microplastics.

It was estimated that approximately 50% of all pipes in the U.S. are repaired using CIPP technology.[88] Based on our current understanding of related microplastic emissions, it is conservatively estimated that approximately 0.25 tons of microplastics are released per CIPP project.[34] However, accurate emission inventories are challenging to provide due to the lack of available statistics on the frequency and scale of the CIPP installations performed.[89] To further advance our understanding of the microplastic emissions during CIPP repair installations, systematic lab-based and field studies are necessary. These studies should explore the scale of microplastics by investigating different resin systems and curing methods to determine their impact on particle composition. Additionally, field monitoring of airborne particle composition throughout the curing process can provide insights into specific points of microplastic release.

The work performed in this study, along with prior research[34,39,63] and potential future studies, is critical for gaining a comprehensive understanding of atmospheric pollution resulting from CIPP repair technology. Obtaining more information about microplastic emissions will enable better comparisons with other sources of urban microplastic pollution. Moreover, this improved understanding will eventually lead to the implementation of improved safety precautions and mitigation regulations to protect the environment and reduce health risks associated with microplastic pollution.

Acknowledgements

This work was supported by the US National Science Foundation, grants CBET-2129166 (A.J.W. group), and CBET-2107946 (A.L. group). The SERS and miniSPLAT analyses were performed at the Environmental Molecular Sciences Laboratory, a National Scientific User Facility sponsored by OBER at PNNL. PNNL is operated by the US Department of Energy by the Battelle Memorial Institute under contract DE-AC06-76RL0. STXM-NEXAFS analyses were performed at beamline 5.3.2 of the Advanced Light Source at Lawrence Berkeley National Laboratory (LBNL), with guidance from M. Marcus and D. Shapiro. LBNL is supported by the Director, Office of Science, Office of Basic Energy Sciences of the US Department of Energy under contract DE-AC02-05CH11231. STXM maps of particles were also acquired at the Canadian Light Source (CLS), with guidance from J. Wang. CLS is supported by the Canada Foundation for Innovation, Natural Sciences and Engineering Research Council of Canada, the University of Saskatchewan, the Government of Saskatchewan, Western Economic

Diversification Canada, the National Research Council Canada and the Canadian Institutes of Health Research.

Author Contributions Statement:

B.N.P. and A.L. developed the analytical framework and experiments for this study. Y.N., P.P., and A.J.W. conducted field studies and provided samples of the CIPP resin, composite, and waste condensate. B.T.O. and P.Z.E. performed SERS analysis. A.Z. performed miniSPLAT data acquisition and analysis. J.M.T., S.A.L.S., F.R.-A, R.C.M., and M.F. assisted with STXM experiments and instrument operation. B.N.P. analyzed SERS and STXM data and collected and analyzed DART-HRMS data with analysis assistance from A.C.M., J.M.T., C.G.W.G, P.E.C, and S.M.H.

Declaration of Interest

The authors declare the following financial interests/personal relationships which may be considered as potential competing interests: AJW is named in a patent application (PCT/US18/28173) filed April 18, 2018, by the Purdue Research Foundation. The patent application pertains to the technologies for capturing, identifying, analyzing, and addressing emissions that are potentially hazardous to the environment and humans. The invention was developed with support from the U.S. National Science Foundation (CBET-1624183).

References

1 R. Geyer, J. R. Jambeck and K. L. Law, Production, use, and fate of all plastics ever made, *Sci. Adv.*, 2017, **3**, e1700782.
2 OECD, Plastics use in 2019, https://www.oecd-ilibrary.org/content/data/efff24eb-en.
3 R. Lehner, C. Weder, A. Petri-Fink and B. Rothen-Rutishauser, Emergence of Nanoplastic in the Environment and Possible Impact on Human Health, *Environ. Sci. Technol.*, 2019, **53**, 1748–1765.
4 M. Cole, P. Lindeque, C. Halsband and T. S. Galloway, Microplastics as contaminants in the marine environment: A review, *Marine Pollution Bulletin*, 2011, **62**, 2588–2597.
5 J. P. G. L. Frias and R. Nash, Microplastics: Finding a consensus on the definition, *Marine Pollution Bulletin*, 2019, **138**, 145–147.
6 J. Gigault, H. El Hadri, B. Nguyen, B. Grassl, L. Rowenczyk, N. Tufenkji, S. Feng and M. Wiesner, Nanoplastics are neither microplastics nor engineered nanoparticles, *Nat. Nanotechnol.*, 2021, **16**, 501–507.

7 N. Joksimovic, D. Selakovic, N. Jovicic, N. Jankovic, P. Pradeepkumar, A. Eftekhari and G. Rosic, Nanoplastics as an Invisible Threat to Humans and the Environment, *Journal of Nanomaterials*, 2022, **2022**, 1–15.

8 J. M. Gonçalves and M. J. Bebianno, Nanoplastics impact on marine biota: A review, *Environmental Pollution*, 2021, **273**, 116426.

9 A. Brewer, I. Dror and B. Berkowitz, The Mobility of Plastic Nanoparticles in Aqueous and Soil Environments: A Critical Review, *ACS EST Water*, 2021, **1**, 48–57.

10 D. Huang, H. Chen, M. Shen, J. Tao, S. Chen, L. Yin, W. Zhou, X. Wang, R. Xiao and R. Li, Recent advances on the transport of microplastics/nanoplastics in abiotic and biotic compartments, *Journal of Hazardous Materials*, 2022, **438**, 129515.

11 Z. Song, X. Yang, F. Chen, F. Zhao, Y. Zhao, L. Ruan, Y. Wang and Y. Yang, Fate and transport of nanoplastics in complex natural aquifer media: Effect of particle size and surface functionalization, *Science of The Total Environment*, 2019, **669**, 120–128.

12 W. Li, B. Zu, Q. Yang, J. Guo and J. Li, Sources, distribution, and environmental effects of microplastics: a systematic review, *RSC Adv.*, 2023, **13**, 15566–15574.

13 A. Facciolà, G. Visalli, M. Pruiti Ciarello and A. Di Pietro, Newly Emerging Airborne Pollutants: Current Knowledge of Health Impact of Micro and Nanoplastics, *IJERPH*, 2021, **18**, 2997.

14 Z. Yang, M. Wang, Z. Feng, Z. Wang, M. Lv, J. Chang, L. Chen and C. Wang, Human Microplastics Exposure and Potential Health Risks to Target Organs by Different Routes: A Review, *Curr Pollution Rep*, 2023, **9**, 468-485. DOI:10.1007/s40726-023-00273-8.

15 A. P. Abad López, J. Trilleras, V. A. Arana, L. S. Garcia-Alzate and C. D. Grande-Tovar, Atmospheric microplastics: exposure, toxicity, and detrimental health effects, *RSC Adv.*, 2023, **13**, 7468–7489.

16 P. Wu, J. Huang, Y. Zheng, Y. Yang, Y. Zhang, F. He, H. Chen, G. Quan, J. Yan, T. Li and B. Gao, Environmental occurrences, fate, and impacts of microplastics, *Ecotoxicology and Environmental Safety*, 2019, **184**, 109612.

17 A. Bianco and M. Passananti, Atmospheric Micro and Nanoplastics: An Enormous Microscopic Problem, *Sustainability*, 2020, **12**, 7327.

18 Y. Zhang, S. Kang, S. Allen, D. Allen, T. Gao and M. Sillanpää, Atmospheric microplastics: A review on current status and perspectives, *Earth-Science Reviews*, 2020, **203**, 103118.

19 S. O'Brien, C. Rauert, F. Ribeiro, E. D. Okoffo, S. D. Burrows, J. W. O'Brien, X. Wang, S. L. Wright and K. V. Thomas, There's something in the air: A review of sources, prevalence and behaviour of microplastics in the atmosphere, *Science of The Total Environment*, 2023, **874**, 162193.

20 S. Gupta, R. Kumar, A. Rajput, R. Gorka, A. Gupta, N. Bhasin, S. Yadav, A. Verma, K. Ram and M. Bhagat, Atmospheric Microplastics: Perspectives on Origin, Abundances, Ecological and Health Risks, *Environ Sci Pollut Res*, 2023, 1-30. DOI:10.1007/s11356-023-28422-y.

21 D. Materić, E. Ludewig, D. Brunner, T. Röckmann and R. Holzinger, Nanoplastics transport to the remote, high-altitude Alps, *Environmental Pollution*, 2021, **288**, 117697.

22 D. Materić, H. A. Kjær, P. Vallelonga, J.-L. Tison, T. Röckmann and R. Holzinger, Nanoplastics measurements in Northern and Southern polar ice, *Environmental Research*, 2022, **208**, 112741.

23 X. Zhao, Y. Zhou, C. Liang, J. Song, S. Yu, G. Liao, P. Zou, K. H. D. Tang and C. Wu, Airborne microplastics: Occurrence, sources, fate, risks and mitigation, *Science of The Total Environment*, 2023, **858**, 159943.

24 J. S. Hanvey, P. J. Lewis, J. L. Lavers, N. D. Crosbie, K. Pozo and B. O. Clarke, A review of analytical techniques for quantifying microplastics in sediments, *Anal. Methods*, 2017, **9**, 1369–1383.

25 W. Wang and J. Wang, Investigation of microplastics in aquatic environments: An overview of the methods used, from field sampling to laboratory analysis, *TrAC Trends in Analytical Chemistry*, 2018, **108**, 195–202.

26 I. Jakubowicz, J. Enebro and N. Yarahmadi, Challenges in the search for nanoplastics in the environment—A critical review from the polymer science perspective, *Polymer Testing*, 2021, **93**, 106953.

27 H. Cai, E. G. Xu, F. Du, R. Li, J. Liu and H. Shi, Analysis of environmental nanoplastics: Progress and challenges, *Chemical Engineering Journal*, 2021, **410**, 128208.

28 W. Zhang, Q. Wang and H. Chen, Challenges in characterization of nanoplastics in the environment, *Front. Environ. Sci. Eng.*, 2022, **16**, 11.

29 L. Xie, K. Gong, Y. Liu and L. Zhang, Strategies and Challenges of Identifying Nanoplastics in Environment by Surface-Enhanced Raman Spectroscopy, *Environ. Sci. Technol.*, 2023, **57**, 25–43.

30 S. Adhikari, V. Kelkar, R. Kumar and R. U. Halden, Methods and challenges in the detection of microplastics and nanoplastics: a mini-review, *Polymer International*, 2022, **71**, 543–551.

31 D. Materić, A. Kasper-Giebl, D. Kau, M. Anten, M. Greilinger, E. Ludewig, E. Van Sebille, T. Röckmann and R. Holzinger, Micro- and Nanoplastics in Alpine Snow: A New Method for Chemical Identification and (Semi)Quantification in the Nanogram Range, *Environ. Sci. Technol.*, 2020, **54**, 2353–2359.

32 D. Materić, R. Holzinger and H. Niemann, Nanoplastics and ultrafine microplastic in the Dutch Wadden Sea – The hidden plastics debris?, *Science of The Total Environment*, 2022, **846**, 157371.

33 N. P. Ivleva, Chemical Analysis of Microplastics and Nanoplastics: Challenges, Advanced Methods, and Perspectives, *Chem. Rev.*, 2021, **121**, 11886–11936.

34 A. C. Morales, J. M. Tomlin, C. P. West, F. A. Rivera-Adorno, B. N. Peterson, S. A. L. Sharpe, Y. Noh, S. M. T. Sendesi, B. E. Boor, J. A. Howarter, R. C. Moffet, S. China, B. T. O'Callahan, P. Z. El-Khoury, A. J. Whelton and A. Laskin, Atmospheric emission of nanoplastics from sewer pipe repairs, *Nat. Nanotechnol.*, 2022, **17**, 1171–1177.

35 R. Sterling, E. Simicevic, E. Allouche, W. Condit and L. Wang, *State of Technology for Rehabilitation of Wastewater Collection Systems*, U.S. Environmental Protection Agency, Washington, D.C., 2010.

36 S. Das, A. Bayat, L. Gay, M. Salimi and J. Matthews, A comprehensive review on the challenges of cured-in-place pipe (CIPP) installations, *Journal of Water Supply: Research and Technology—AQUA*, 2016, **65**, 583–596.

37 S. M. Teimouri Sendesi, K. Ra, E. N. Conkling, B. E. Boor, Md. Nuruddin, J. A. Howarter, J. P. Youngblood, L. M. Kobos, J. H. Shannahan, C. T. Jafvert and A. J. Whelton, Worksite Chemical Air Emissions and Worker Exposure during Sanitary Sewer and Stormwater Pipe Rehabilitation Using Cured-in-Place-Pipe (CIPP), *Environ. Sci. Technol. Lett.*, 2017, **4**, 325–333.

38 Y. Noh, T. Odimayomi, S. M. Teimouri Sendesi, J. P. Youngblood and A. J. Whelton, Environmental and human health risks of plastic composites can be reduced by optimizing manufacturing conditions, *Journal of Cleaner Production*, 2022, **356**, 131803.

39 A. C. Morales, J. M. Tomlin, B. N. Peterson, F. A. Rivera-Adorno, S. A. L. Sharpe, S. Huston, Y. Noh, S. M. T. Sendesi, B. E. Boor, J. A. Howarter, R. C. Moffet, S. China, A. J. Whelton and A. Laskin, Single-Particle analysis of Nanoplastic Particles from Sewage Pipe Repair. Submitted to *Aerosol Science and Technology.*

40 Wiley Science Solutions, *WileyKnowItAll*.

41 G. Schoukens, J. Martins and P. Samyn, Insights in the molecular structure of low- and high-molecular weight poly(styrene-maleic anhydride) from vibrational and resonance spectroscopy, *Polymer*, 2013, **54**, 349–362.

42 C. May, *Epoxy resins: chemistry and technology*, Routledge, 2018.

43 R. Ullah and Y. Zheng, Raman spectroscopy of 'Bisphenol A', *Journal of Molecular Structure*, 2016, **1108**, 649–653.

44 R. C. Moffet, T. R. Henn, A. V. Tivanski, R. J. Hopkins, Y. Desyaterik, A. L. D. Kilcoyne, T. Tyliszczak, J. Fast, J. Barnard, V. Shutthanandan, S. S. Cliff, K. D. Perry, A. Laskin and M. K. Gilles, Microscopic

characterization of carbonaceous aerosol particle aging in the outflow from Mexico City, *Atmos. Chem. Phys.*, 2010, **10**, 961–976.

45 R. C. Moffet, T. C. Rödel, S. T. Kelly, X. Y. Yu, G. T. Carroll, J. Fast, R. A. Zaveri, A. Laskin and M. K. Gilles, Spectro-microscopic measurements of carbonaceous aerosol aging in Central California, *Atmos. Chem. Phys.*, 2013, **13**, 10445–10459.

46 R. C. Moffet, R. E. O'Brien, P. A. Alpert, S. T. Kelly, D. Q. Pham, M. K. Gilles, D. A. Knopf and A. Laskin, Morphology and mixing of black carbon particles collected in central California during the CARES field study, *Atmos. Chem. Phys.*, 2016, **16**, 14515–14525.

47 M. Fraund, T. Park, L. Yao, D. Bonanno, D. Q. Pham and R. C. Moffet, Quantitative capabilities of STXM to measure spatially resolved organic volume fractions of mixed organic ⁄ inorganic particles, *Atmos. Meas. Tech.*, 2019, **12**, 1619–1633.

48 J. M. Tomlin, K. A. Jankowski, F. A. Rivera-Adorno, M. Fraund, S. China, B. H. Stirm, R. Kaeser, G. S. Eakins, R. C. Moffet, P. B. Shepson and A. Laskin, Chemical Imaging of Fine Mode Atmospheric Particles Collected from a Research Aircraft over Agricultural Fields, *ACS Earth Space Chem.*, 2020, **4**, 2171–2184.

49 A. Zelenyuk, D. Imre, J. Wilson, Z. Zhang, J. Wang and K. Mueller, Airborne Single Particle Mass Spectrometers (SPLAT II & miniSPLAT) and New Software for Data Visualization and Analysis in a Geo-Spatial Context, *J. Am. Soc. Mass Spectrom.*, 2015, **26**, 257–270.

50 R. B. Cody, J. A. Laramee, J. M. Nilles and H. D. Durst, Direct analysis in real time (DART) mass spectrometry, *JEOL news*, 2005, **40**, 8–12.

51 M. Marić, J. Marano, R. B. Cody and C. Bridge, DART-MS: A New Analytical Technique for Forensic Paint Analysis, *Anal. Chem.*, 2018, **90**, 6877–6884.

52 V. L. Benefield, S. Perna, S. Pham, N. S. Chong, Z. Li and M. Zhang, Evaluation of Mass Spectrometric Methods for Screening Polycyclic Aromatic Hydrocarbons in the Particulate Phase of Wildfire/Biomass Smoke, *Fire Technol*, 2023. DOI:10.1007/s10694-022-01327-x.

53 C. P. West, Y.-J. Hsu, K. T. MacFeely, S. M. Huston, B. P. Aridjis-Olivos, A. C. Morales and A. Laskin, Volatility Measurements of Individual Components in Organic Aerosol Mixtures Using Temperature-Programmed Desorption–Direct Analysis in Real Time–High Resolution Mass Spectrometry, *Anal. Chem.*, 2023, **95**, 7403–7408.

54 D. B. Priddy, in *Polymer Synthesis*, Springer-Verlag, Berlin/Heidelberg, 1994, vol. 111, pp. 67–114.

55 K. Ra, S. M. Teimouri Sendesi, Md. Nuruddin, N. N. Zyaykina, E. N. Conkling, B. E. Boor, C. T. Jafvert, J. A. Howarter, J. P. Youngblood and A. J. Whelton, Considerations for emission monitoring and liner analysis of thermally manufactured sewer cured-in-place-pipes (CIPP), *Journal of Hazardous Materials*, 2019, **371**, 540–549.

56 Moffet, R. C.; Tivanski, A. V.; Gilles, M. K. Scanning X-ray Transmission Microscopy: Applications in Atmospheric Aerosol Research. In Fundamentals and Applications in Aerosol Spectroscopy; Signorell, R., Reid, J. P., Eds.; Taylor and Francis Books, Inc., 2010; pp 419−462.

57 R. C. Moffet, T. Henn, A. Laskin and M. K. Gilles, Automated Chemical Analysis of Internally Mixed Aerosol Particles Using X-ray Spectromicroscopy at the Carbon K-Edge †, *Anal. Chem.*, 2010, **82**, 7906–7914.

58 C. Bridge and M. Marić, Temperature-Dependent DART-MS Analysis of Sexual Lubricants to Increase Accurate Associations, *J. Am. Soc. Mass Spectrom.*, 2019, **30**, 1343–1358.

59 R. B. Cody, T. N. J. Fouquet and C. Takei, Thermal desorption and pyrolysis direct analysis in real time mass spectrometry for qualitative characterization of polymers and polymer additives, *Rapid Commun Mass Spectrom*, 2020, **34**, S2. DOI:10.1002/rcm.8687.

60 J. H. Gross, Direct analysis in real time—a critical review on DART-MS, *Anal Bioanal Chem*, 2014, **406**, 63–80.

61 X. Zhang, A. Mell, F. Li, C. Thaysen, B. Musselman, J. Tice, D. Vukovic, C. Rochman, P. A. Helm and K. J. Jobst, Rapid fingerprinting of source and environmental microplastics using direct analysis in real time-high resolution mass spectrometry, *Analytica Chimica Acta*, 2020, **1100**, 107–117.

62 M. Velimirovic, K. Tirez, S. Verstraelen, E. Frijns, S. Remy, G. Koppen, A. Rotander, E. Bolea-Fernandez and F. Vanhaecke, Mass spectrometry as a powerful analytical tool for the characterization of indoor airborne microplastics and nanoplastics, *J. Anal. At. Spectrom.*, 2021, **36**, 695–705.

63 A. C. Morales, C. P. West, B. N. Peterson, Y. Noh, A. J. Whelton and A. Laskin, Diversity of Organic Components in Airborne Waste Discharged from Sewer Pipe Repairs, *Environ. Sci.: Processes Impacts*, 2023, 10.1039.D3EM00084B.

64 B. Kirchsteiger, D. Materić, F. Happenhofer, R. Holzinger and A. Kasper-Giebl, Fine micro- and nanoplastics particles (PM2.5) in urban air and their relation to polycyclic aromatic hydrocarbons, *Atmospheric Environment*, 2023, **301**, 119670.

65 M. L. Tabor, D. Newman and A. J. Whelton, Stormwater Chemical Contamination Caused by Cured-in-Place Pipe (CIPP) Infrastructure Rehabilitation Activities, *Environ. Sci. Technol.*, 2014, **48**, 10938–10947.

66 S. M. Teimouri Sendesi, Y. Noh, M. Nuruddin, B. E. Boor, J. A. Howarter, J. P. Youngblood, C. T. Jafvert and A. J. Whelton, An emerging mobile air pollution source: outdoor plastic liner manufacturing sites discharge VOCs into urban and rural areas, *Environ. Sci.: Processes Impacts*, 2020, **22**, 1828–1841.

67 S. Kim, R. W. Kramer and P. G. Hatcher, Graphical Method for Analysis of Ultrahigh-Resolution Broadband Mass Spectra of Natural Organic Matter, the Van Krevelen Diagram, *Anal. Chem.*, 2003, **75**, 5336–5344.

68 I. J. George and J. P. D. Abbatt, Heterogeneous oxidation of atmospheric aerosol particles by gas-phase radicals, *Nature Chemistry*, 2010, **2**, 713–722.

69 J. H. Kroll and J. H. Seinfeld, Chemistry of secondary organic aerosol: Formation and evolution of low-volatility organics in the atmosphere, *Atmospheric Environment*, 2008, **42**, 3593–3624.

70 Y. Li, U. Pöschl and M. Shiraiwa, Molecular corridors and parameterizations of volatility in the chemical evolution of organic aerosols, *Atmos. Chem. Phys.*, 2016, **16**, 3327–3344.

71 W.-S. W. DeRieux, Y. Li, P. Lin, J. Laskin, A. Laskin, A. K. Bertram, S. A. Nizkorodov and M. Shiraiwa, Predicting the glass transition temperature and viscosity of secondary organic material using molecular composition, *Atmos. Chem. Phys.*, 2018, **18**, 6331–6351.

72 J. Laskin, A. Laskin, S. A. Nizkorodov, P. Roach, P. Eckert, M. K. Gilles, B. Wang, H. J. (Julie) Lee and Q. Hu, Molecular Selectivity of Brown Carbon Chromophores, *Environ. Sci. Technol.*, 2014, **48**, 12047–12055.

73 H. Herrmann, T. Schaefer, A. Tilgner, S. A. Styler, C. Weller, M. Teich and T. Otto, Tropospheric Aqueous-Phase Chemistry: Kinetics, Mechanisms, and Its Coupling to a Changing Gas Phase, *Chem. Rev.*, 2015, **115**, 4259–4334.

74 R. Zhao, A. K. Y. Lee, R. Soong, A. J. Simpson and J. P. D. Abbatt, Formation of aqueous-phase α-hydroxyhydroperoxides (α-HHP): potential atmospheric impacts, *Atmos. Chem. Phys.*, 2013, **13**, 5857–5872.

75 T. B. Nguyen, P. J. Roach, J. Laskin, A. Laskin and S. A. Nizkorodov, Effect of humidity on the composition of isoprene photooxidation secondary organic aerosol, *Atmos. Chem. Phys.*, 2011, **11**, 6931–6944.

76 P. J. Ziemann, Formation of Alkoxyhydroperoxy Aldehydes and Cyclic Peroxyhemiacetals from Reactions of Cyclic Alkenes with O_3 in the Presence of Alcohols, *J. Phys. Chem. A*, 2003, **107**, 2048–2060.

77 H. Kimura, A simple method for the anionic polymerization of ?-carbonyl acids in water, *J. Polym. Sci. A Polym. Chem.*, 1998, **36**, 189–193.

78 J. P. Reid, A. K. Bertram, D. O. Topping, A. Laskin, S. T. Martin, M. D. Petters, F. D. Pope and G. Rovelli, The viscosity of atmospherically relevant organic particles, *Nat Commun*, 2018, **9**, 956.

79 R. Schmedding, Q. Z. Rasool, Y. Zhang, H. O. T. Pye, H. Zhang, Y. Chen, J. D. Surratt, F. D. Lopez-Hilfiker, J. A. Thornton, A. H. Goldstein and W. Vizuete, Predicting secondary organic aerosol phase state and viscosity and its effect on multiphase chemistry in a regional-scale air quality model, *Atmos. Chem. Phys.*, 2020, **20**, 8201–8225.

80 L. Xia, Y. Noh, A. J. Whelton, B. E. Boor, B. Cooper, N. I. Lichti, J. H. Park and J. H. Shannahan, Pulmonary and neurological health effects associated with exposure to representative composite manufacturing emissions and corresponding alterations in circulating metabolite profiles, *Toxicological Sciences*, 2023, **193**, 62-79.

81 T. Koop, J. Bookhold, M. Shiraiwa and U. Pöschl, Glass transition and phase state of organic compounds: dependency on molecular properties and implications for secondary organic aerosols in the atmosphere, *Phys. Chem. Chem. Phys.*, 2011, **13**, 19238.

82 M. Shiraiwa, M. Ammann, T. Koop and U. Pöschl, Gas uptake and chemical aging of semisolid organic aerosol particles, *Proc. Natl. Acad. Sci. U.S.A.*, 2011, **108**, 11003–11008.

83 T. Berkemeier, S. S. Steimer, U. K. Krieger, T. Peter, U. Pöschl, M. Ammann and M. Shiraiwa, Ozone uptake on glassy, semi-solid and liquid organic matter and the role of reactive oxygen intermediates in atmospheric aerosol chemistry, *Phys. Chem. Chem. Phys.*, 2016, **18**, 12662–12674.

84 P. J. DeMott, A. J. Prenni, X. Liu, S. M. Kreidenweis, M. D. Petters, C. H. Twohy, M. S. Richardson, T. Eidhammer and D. C. Rogers, Predicting global atmospheric ice nuclei distributions and their impacts on climate, *Proceedings of the National Academy of Sciences*, 2010, **107**, 11217–11222.

85 M. Aeschlimann, G. Li, Z. A. Kanji and D. M. Mitrano, Potential impacts of atmospheric microplastics and nanoplastics on cloud formation processes, *Nat. Geosci.*, 2022, **15**, 967–975.

86 B. Zobrist, C. Marcolli, D. A. Pedernera and T. Koop, Do atmospheric aerosols form glasses?, *Atmospheric Chemistry and Physics*, 2008, **8**, 5221–5244.

87 P. Ebrahimi, S. Abbasi, R. Pashaei, A. Bogusz and P. Oleszczuk, Investigating impact of physicochemical properties of microplastics on human health: A short bibliometric analysis and review, *Chemosphere*, 2022, **289**, 133146.

88 A. J. Whelton, J. Shannahan, B. E. Boor, J. A. Howarter, J. P. Youngblood and C. T. Jafvert, Cured-in-Place-Pipe (CIPP): Inhalation and Dermal Exposure Risks Associated with Sanitary Sewer, Storm Sewer, and Drinking Water Pipe Repairs, 2017, https://blogs.cdc.gov/niosh-science-blog/2017/09/26/cipp/, (accessed 17 July 2023).

89 C.-Y. Chen, T.-H. Lu, W.-M. Wang and C.-M. Liao, Assessing regional emissions of vehicle-based tire wear particle from macro-to micro/nano-scales with pandemic lockdowns and electromobility scenarios implications, *Chemosphere*, 2023, **311**, 137209.